Performance Predictions for Isolators and Differential Phase Shifters for the Near-Millimeter Wave Range

SALVADOR H. TALISA, MEMBER, IEEE, AND DONALD M. BOLLE, SENIOR MEMBER, IEEE

Abstract—**An analytical and numerical study is presented for a five-region planar canonical structure modeling quasi-optical integrated surface magnetoplasmon based nonreciprocal devices for the near-millimeter wave range. The model includes a slab of a high quality semiconducting material, such as n-GaAs, magnetized parallel to its surfaces and perpendicular to the direction of propagation.**

The analysis performed is exact. Sample results show the possibility of acceptable performance for isolators over a bandwidth of 45 GHz in the 500-GHz range and of differential phase shifter design over a bandwidth of 65 GHz in the 380-GHz range.

List of Symbols

ω	Angular frequency (rad/s).
ω_p	Plasma frequency (rad/s) $\frac{ne^2}{\epsilon_0 m^*}$.
ω_c	Cyclotron frequency (rad/s) $\frac{eB_0}{m^*}$.
n	Carrier concentration (m^{-3}).
e	Electron charge (C).
m^*	Electron effective mass (kg) 0.067 m_e (for GaAs).
m_e	Electron rest mass (kg).
B_0	DC magnetizing field (Wb/m^2).
ϵ_0, μ_0	Vacuum permittivity and permeability, respectively.
$\epsilon^{(0)}$	Static dielectric constant of the semiconducting material 12.95 (for GaAs).
ν	Collision frequency (rad/s) $1/\tau$.
τ	Momentum relaxation time of the semiconducting material.
γ	Complex propagation constant $\alpha + j\beta$.
α	Attenuation constant.
β	Phase constant.
k_i	Transverse wavenumber of the ith region.
ϵ_i	Relative dielectric constant of the ith region.
$\epsilon_e(\omega)$	Effective relative dielectric constant of the semiconducting medium ($\epsilon_e(\omega) \equiv \epsilon_2$).
D_1, D_2, D_3	Widths of the slab regions.

Manuscript received April 13, 1981; revised August 3, 1981. This work was supported by the U.S. Navy, Office of Naval Research, under Contract N00014-80-C-0982.

The authors are with the Department of Electrical and Computer Engineering, Lehigh University, Packard Laboratory #19, Bethelehem, PA 18015.

I. Introduction

IN THIS paper we present the results of a study which is aimed at developing a fundamental understanding of surface magnetoplasmons on high quality semiconducting substrates. The information obtained will have direct application in the design of quasi-optical integrated nonreciprocal devices in the near-millimeter wave range, such as isolators, phase shifters, and circulators.

Theoretical and experimental studies on nonreciprocal devices for the millimeter through infrared wave ranges employing magnetoplasmas have been carried out by May *et al.* [3]–[7]. Important contributions to this field are also the works by Jacobs and Chrepta [8] on millimeter wave phase shifters and by Eberhardt *et al.* [9] on quasi-optical wave propagation in gyromagnetic and gyroelectric media.

In the study presented here, design considerations and performance predictions are based on the analysis of multilayer canonical structures of up to five regions including a slab of a high quality doped semiconductor. In this work we have considered n-type GaAs with a carrier concentration equivalent to a plasma frequency $\omega_p = 10^{13}$ rad/s ($n = 2.1 \times 10^{15}$ electrons/cm^3). Losses in the GaAs slab are modeled using momentum relaxation times of the order of $\tau = 8 \times 10^{-12}$ s [1].

A uniform magnetic field is applied parallel to the GaAs slab surfaces and perpendicular to the direction of propagation (Fig. 1) yielding a cyclotron frequency $\omega_c = 10^{12}$ rad/s ($B_0 = 3810$ G). This value has been used throughout the calculations presented here. The resultant anisotropic medium is characterized by the complex permittivity tensor [1] given in Section II.

As has been discussed elsewhere [1], [2], waves propagating in a slab of GaAs material exhibit a field displacement effect when exposed to a uniform dc magnetic field. In addition, we observe nonreciprocal propagation characteristics for semiconducting slabs which are asymmetrically loaded.

The modeling of quasi-optical integrated nonreciprocal devices by multilayer canonical structures naturally fits into the effective dielectric constant method first introduced by Knox and Toulios [10], based on Marcatili's

0018-9480/81/1200-1338$00.75

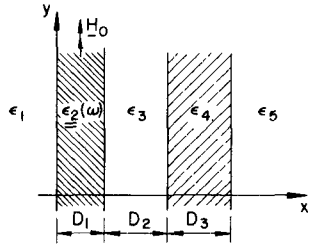

Fig. 1. Five-region canonical structure.

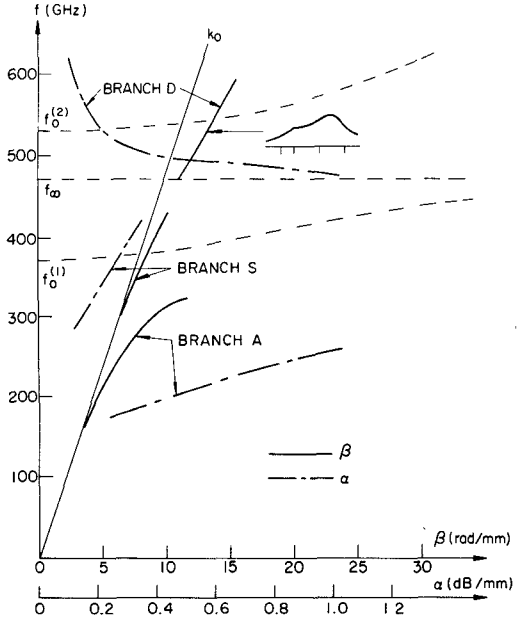

Fig. 2. Sample dispersion diagram for the five-region canonical structure. Nonreciprocal device isolation. Forward propagation. Parameters: $\omega_p = 10^{13}$, $\omega_c = 10^{12}$, $\tau = 8 \times 10^{-12}$, $\epsilon^{(0)} = 13$, $\epsilon_4 = 4$, $\epsilon_1 = \epsilon_3 = \epsilon_5 = 1$, $D_1 = 50$ μm, $D_2 = D_3 = 100$ μm.

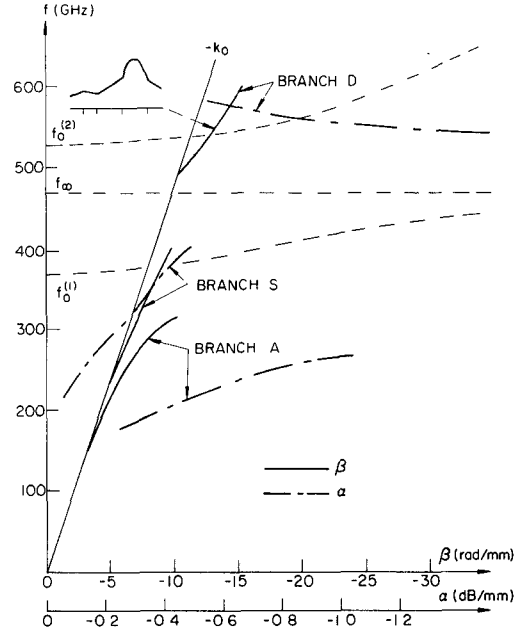

Fig. 3. Sample dispersion diagram for the five-region canonical structure. Nonreciprocal device isolation. Reverse propagation. Parameters as for Fig. 2.

approximate analysis [11] of rectangular dielectric waveguides. The method was further developed by Itoh and Mittra [12] and is employed in the analysis of different rectangular dielectric waveguiding structures suitable for use in millimeter wave through optical integrated circuits.

Thus the five-region model considered here, consisting of a dielectric slab parallel to the semiconducting slab and placed at a certain distance from it, is appropriate for the modeling of two rectangular dielectric waveguides embedded in a dielectric substrate, one of which is the semiconducting material.

Planar canonical structures modeling millimeter wave ferrite based nonreciprocal devices have also been used by Itoh [13].

The results presented here for gyroelectric materials have their gyromagnetic counterpart in those obtained for planar ferrite loaded microwave devices [14]–[17] (see also [13]), although the reasons for modeling microstrip and stripline ferrite devices with multilayer canonical structures are different to those for quasi-optical devices. However, magnetized semiconducting slabs offer a greater wealth of modes that display the field displacement effect.

This is because, within the range of interest, the semiconductor effective permittivity becomes negative in two separate frequency intervals, i.e., for $0 < \omega < \omega_0^{(1)}$ and $\omega_\infty < \omega < \omega_0^{(2)}$ [1]. Thus for a magnetized GaAs slab, branches A and S (see Figs. 2 and 3) are found in the first interval, while branches D and E are obtained in the second. These four branches exhibit field displacement effects [1], [2].

On the other hand, the effective permeability of magnetized ferrite slabs is negative only in one frequency interval [16], with a functional dependence similar to that of the effective dielectric constant of GaAs between ω_∞ and $\omega_0^{(2)}$. Indeed, branches D and E resemble the dynamic and magnetostatic modes found for ferrites [14]–[17].

In Section II of this article, a brief account is given of the theoretical analysis made for the five-region geometry. The analysis performed is exact. In Section III the results of this analysis are presented. Typical dispersion and loss diagrams are given which show encouraging device isolation and phase shifting characteristics.

An important achievement in connection with our computations was the utilization of a very reliable and efficient algorithm based on Davidenko's method [18], [19] used to

find the complex roots of the complex dispersion relation for the system.

II. Theory

The geometry to be analyzed is shown in Fig. 1. It is assumed to be infinite in the y-direction. Regions 1 and 5 extend to $x \to -\infty$ and $x \to +\infty$, respectively. Region 2 is the semiconducting material while regions 1, 3, 4, and 5 are dielectric regions with different permittivities. Propagation of the electromagnetic fields is in the z-direction.

For a uniform dc magnetizing field, as shown in Fig. 1, the semiconductor dielectric tensor takes the form

$$\epsilon(\omega)=\begin{bmatrix} \xi & 0 & -j\eta \\ 0 & \zeta & 0 \\ j\eta & 0 & \xi \end{bmatrix} \tag{1}$$

where

$$\xi=\epsilon^{(0)}-\frac{\omega_p^2(\omega-j\nu)}{\omega\left[(\omega-j\nu)^2-\omega_c^2\right]} \tag{2}$$

$$\eta=\frac{-\omega_p^2\omega_c}{\omega\left[(\omega-j\nu)^2-\omega_c^2\right]} \tag{3}$$

$$\zeta=\epsilon^{(0)}-\frac{\omega_p^2}{\omega(\omega-j\nu)}. \tag{4}$$

The different parameters involved and the notation employed in (1) to (4) are listed in the nomenclature.

Only TM modes are considered here since fields corresponding to TE modes do not exhibit interesting interactions with the semiconducting material. For an infinite structure in the y-direction only three field components result: H_y, E_x, and E_z.

We restrict our consideration to the bounded modes of the structure, i.e., those for which the fields decay exponentially in the transverse direction.

Solution of Maxwell's equations, with the boundary conditions appropriate to the geometry given in Fig. 1, leads to a complex transcendental equation whose complex roots yield the propagation constants (i.e., $\gamma=\alpha+j\beta$) characteristic of this waveguiding system. This transcendental equation or dispersion relation is given below. The notation employed is shown in the list of symbols.

$$F(\omega;\gamma)=e^{-2k_2D_1}-\frac{e^{k_4D_3}\left(R_1e^{k_3D_2}+R_2e^{-k_3D_2}\right)+e^{-k_4D_3}\left(R_3e^{k_3D_2}+R_4e^{-k_3D_2}\right)}{e^{k_4D_3}\left(R_5e^{k_3D_2}+R_6e^{-k_3D_2}\right)+e^{-k_4D_3}\left(R_7e^{k_3D_2}+R_8e^{-k_3D_2}\right)}=0 \tag{5}$$

where

$$k_i^2=-\gamma^2-k_0^2\epsilon_i; \quad i=1,3,4,5 \tag{6}$$

$$k_2^2=-\gamma^2-k_0^2\epsilon_e(\omega) \tag{7}$$

with

$$\epsilon_e(\omega)=\frac{\xi^2-\eta^2}{\xi} \tag{8}$$

$$k_0^2=\omega^2\mu_0\epsilon_0. \tag{9}$$

The coefficients R_1 to R_8 are obtained from the function

$$R(\mathfrak{k},\mathfrak{l},\mathfrak{m},\mathfrak{n},\mathfrak{p},\mathfrak{q}) = \left(\frac{k_4}{\epsilon_4}+\mathfrak{k}\frac{k_5}{\epsilon_5}\right)\left(\frac{k_3}{\epsilon_3}+\mathfrak{l}\frac{k_4}{\epsilon_4}\right)\left(k_2+\mathfrak{m}\,j\gamma\frac{\eta}{\xi}+\mathfrak{n}\epsilon_e\frac{k_3}{\epsilon_3}\right) \cdot\left(k_2+\mathfrak{p}\,j\gamma\frac{\eta}{\xi}+\mathfrak{q}\epsilon_e\frac{k_1}{\epsilon_1}\right) \tag{10}$$

in the following way:

$$\begin{aligned} R_1&=R(1,1,-1,1,1,1) & R_5&=R(1,1,1,-1,-1,-1)\\ R_2&=R(1,-1,-1,-1,1,1) & R_6&=R(1,-1,1,1,-1,-1)\\ R_3&=R(-1,-1,-1,1,1,1) & R_7&=R(-1,-1,1,-1,-1,-1)\\ R_4&=R(-1,1,-1,-1,1,1) & R_8&=R(-1,1,1,1,-1,-1). \end{aligned}$$

Throughout these calculations, a time dependence factor $e^{j\omega t}$ and a propagation factor $e^{-\gamma z}$ have been assumed.

Equation (5), when solved for different values of ω, gives the modal spectrum of the configuration. Typical examples are given in Figs. 2 and 3.

As mentioned in Section I, (5) is solved using an algorithm based on Davidenko's method. This method consists of reducing the Newton–Raphson iterative procedure to a set of simultaneous first-order differential equations in a dummy variable. This system is then solved numerically using the subroutine RKF45 [20], [21].

This algorithm has proven to be very efficient and reliable.

III. Nonreciprocal Device Behavior

Typical loss and dispersion diagrams showing the modal spectrum for the five-region model are given in Figs. 2 and 3 for the configuration shown in Fig. 1. The different branches shown can be compared with those obtained for the single GaAs slab [1], [2]. Branch E is heavily attenuated and is not shown in Figs. 2 and 3.

Since the GaAs is the lossiest material in the guiding system, the energy must be preferentially guided outside the semiconducting slab. The reason for modeling quasi-optical integrated nonreciprocal devices using a five-region planar geometry is that it allows us to vary the structure parameters so as to control the fraction of energy which is

TABLE I
ISOLATION (SEE FIGS. 2 AND 3)

$\omega(\times 10^{12})$	f(GHz)	Insertion Loss dB/mm	Insertion Loss dB/λ_g	Isolation dB/mm	Isolation dB/λ_g
3.0	477	0.96	0.55	∞	-
3.1	493	0.52	0.27	∞	-
3.2	509	0.30	0.15	3.6	1.98
3.3	525	0.26	0.12	2.6	1.34
3.4	541	0.18	0.08	1.6	0.77

TABLE II
PHASE SHIFT (SEE FIGS. 4 AND 5)

			Insertion loss (dB/mm)					
			$\tau = 20 \times 10^{-12}$		$\tau = 15 \times 10^{-12}$		$\tau = 10 \times 10^{-12}$	
$\omega(\times 10^{-12})$	f(GHz)	$\Delta\phi$(°/mm)	$H_o > 0$	$H_o < 0$	$H_o > 0$	$H_o < 0$	$H_o > 0$	$H_o < 0$
2.2	350	80	0.23	0.76	0.32	1.02	0.48	1.53
2.3	366	97	0.34	0.61	0.47	0.80	0.70	1.18
2.4	382	109	0.45	0.53	0.60	0.70	0.90	1.03
2.5	398	120	0.55	0.57	0.75	0.76	1.09	1.15
2.6	414	120	0.65	0.77	0.87	1.03	1.29	1.53

carried external to the semiconducting slab, as well as the amount of dielectric loading on one side of the GaAs slab.

The semiconducting slab is then required only to the extent that it introduces sufficient nonreciprocity in the propagation characteristics. In the case of an isolator, it is desired that, making use of the field displacement effect, most of the energy travels within the GaAs slab for one direction of propagation (thus suffering considerable attenuation) while for the other propagation direction the energy is predominantly carried by the second dielectric slab, region 4.

It must be added that, for differential phase shifters, significant nonreciprocal phase shifts at highly desirable values of the insertion loss are obtained for relaxation times (τ) higher than those currently available.

A. Nonreciprocal Device Isolation

Branch D, in Figs. 2 and 3, offers nonreciprocal characteristics which can be used for isolator design. The data shown in Table I, taken from these figures, shows that device isolation can be obtained over a bandwidth of about 45 GHz—in the 500-GHz range ($\lambda_0 = 0.6$ mm)—with an insertion loss of 0.5 dB/mm or less, and an isolation ratio of 10:1 or better. For somewhat higher insertion losses and lower isolation ratios, this bandwidth could be extended to 60 or 70 GHz. (It must be noted that branch D has its onset at $\omega = 2.95 \times 10^{12}$ rad/s in the forward propagation direction.)

The mechanism through which nonreciprocal isolation is obtained can be understood from the field distributions for branch D, an example of which is given in Figs. 2 and 3. For the forward propagation direction the fields adhere to the high dielectric loaded side of the GaAs slab, the dielectric slab thus guiding the energy away from the semiconductor. This effect is achieved more efficiently toward the higher end of the band where the attenuation is thus lowest.

For the reverse propagation, at lower frequencies the electromagnetic energy concentrates more heavily in the vicinity of the air–GaAs interface opposite to the dielectric slab. Due to the influence of the latter, then, more energy is forced to travel within the GaAs and is therefore attenuated. This effect diminishes as the frequency increases.

B. Nonreciprocal Phase Shifting

Figs. 4 and 5 show modes S and A for the configuration given in the insert. In this case, branch S exhibits characteristics that are suitable for differential phase shifter design over a bandwidth that strongly depends upon the loss parameter τ of the semiconducting region. This information can be obtained directly from Figs. 4 and 5 and is summarized in Table II.

Thus if the semiconducting material is assumed to have a relaxation time of $\tau = 20 \times 10^{-12}$ s, substantial differential phase shifts (between 80 and 120°/mm) with a maximum insertion loss of 0.76 dB/mm can be obtained for a

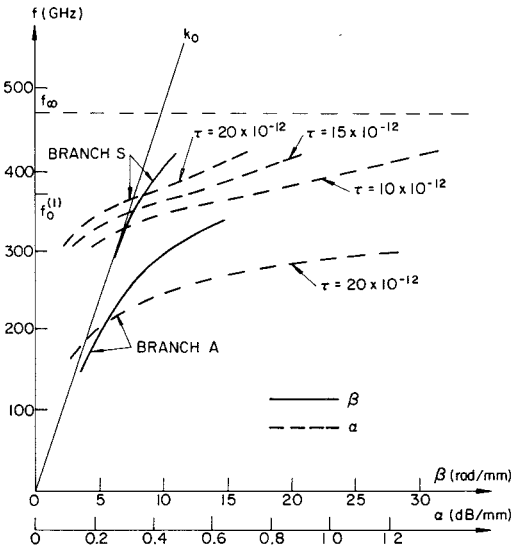

Fig. 4. Branch S: differential phase shift. Forward propagation. Parameters: $\omega_p = 10^{13}$, $\omega_c = 10^{12}$, $\epsilon^{(0)} = 13$, $\epsilon_4 = 6$, $\epsilon_1 = \epsilon_3 = \epsilon_5 = 1$, $D_1 = 75$ μm, $D_2 = 50$ μm, $D_3 = 100$ μm.

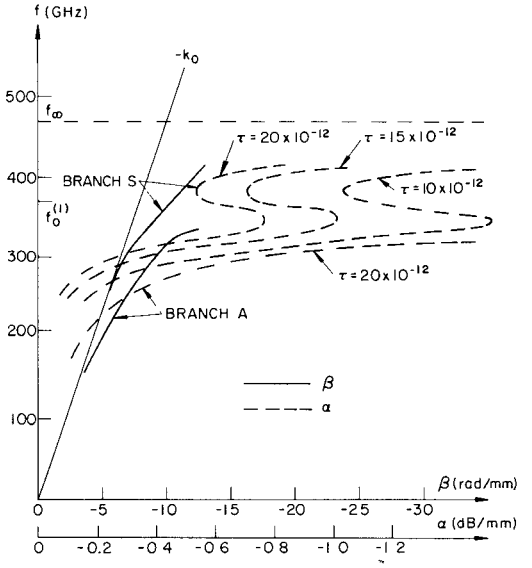

Fig. 5. Branch S: differential phase shift. Reverse propagation. Parameters as for Fig. 4.

bandwidth of about 65 GHz in the 380-GHz range ($\lambda_0 = 0.8$ mm). For $\tau = 15 \times 10^{-2}$ s the bandwidth is reduced to about 30 GHz with differential phase shifts between 97 and 120°/mm for the same maximum insertion loss as above.

As can be seen from Table II, for values of τ of the order of 10×10^{-12} s or lower, the insertion loss increases beyond 1 dB/mm.

It should be noted, from Figs. 4 and 5, that branch A is highly attenuated at the frequencies of interest and plays no role.

Within this range, for the forward propagation direction (or, equivalently, for positive biasing magnetic field) an important portion of the energy travels in region 1. This is indicated in Fig. 4 by the proximity of branch S to the light line in vacuum ($\epsilon_1 = 1$).

For the reverse propagation direction (or for negative biasing magnetic field), a phenomenon already studied in [1] occurs. The fields, which at lower frequencies adhere to the low dielectric side of the GaAs slab, change their distribution within a short frequency range, concentrating now in the vicinity of the opposite air–GaAs interface ($\epsilon_3 = 1$). In this transition band, more energy travels within the semiconducting slab, hence the attenuation peak obtained at around 350 GHz (Fig. 5). Once this transition is completed, the fields again travel mostly outside the GaAs, thus experiencing lower attenuation. As the frequency increases, however, losses also increase since branch S gradually becomes a "volume" mode [1].

This feature of branch S has been fully explained in [1],

where a single semiconducting slab with maximum asymmetric loading is considered, that is, sided by semi-infinite media of different dielectric constants.

IV. Conclusion

The results of an analytical and numerical investigation have been presented for structures modeling quasi-optical integrated nonreciprocal devices for the near-millimeter wave range based on surface magnetoplasmons. The model is a canonical multilayer structure which includes a slab of high quality semiconducting material such as n-type GaAs, exposed to a uniform dc magnetic field parallel to its surfaces and perpendicular to the direction of propagation.

The study of the five-region geometry presented here is suitable for the analysis of rectangular dielectric waveguiding structures through the use of the effective dielectric constant method.

The analysis performed is exact. Results obtained show loss and dispersion characteristics which are encouraging for isolators and phase shifters. Thus an isolation ratio of 10:1 over a bandwidth of 45 GHz in the 500-GHz range is shown to be achievable.

Regarding phase shifters, our results show a strong dependence on the loss parameter of the semiconductor. Furthermore, phase shifter characteristics which match those at microwave frequencies are possible provided the quality of the semiconducting material can be improved. Thus significant phase shifts (80 to 120°/mm) at desirable insertion losses are obtained for relaxation times of the order of 20×10^{-12} s over a bandwidth of 65 GHz in the 380-GHz range. This bandwidth is reduced by half when $\tau=15\times10^{-12}$ s. These values of the momentum relaxation time are significantly higher than those currently available ($\tau\leq8\times10^{-12}$ s) for GaAs. At this point, other III–V materials appear to offer greater promise for the attaining of the desired relaxation times.

References

[1] D. M. Bolle and S. H. Talisa, "Fundamental considerations in millimeter and submillimeter component design employing magnetoplasmons," *IEEE Trans. Microwave Theory Tech.*, vol. MTT-29, Sept. 1981.

[2] S. H. Talisa and D. M. Bolle, "Performance characteristics of magnetoplasmon based submillimeter wave nonreciprocal devices," in *IEEE MTT-S Int. Microwave Symp. Dig.*, pp. 287–289, 1981.

[3] R. E. Hayes and W. G. May, "The use of semiconductors in nonreciprocal devices for submillimeter wavelengths," in *Proc. Symp. on Submillimeter Waves*, Polytechnic Inst. of Brooklyn, pp. 237–250, 1970.

[4] B. R. McLeod and W. G. May, "A 35 GHz isolator using a coaxial solid-state plasma in a longitudinal magnetic field," *IEEE Trans. Microwave Theory Tech.*, vol. MTT-19, pp. 510–516, June 1971.

[5] M. Kanda and W. G. May, "Nonreciprocal reflection-beam isolators for far-infrared use," *IEEE Trans. Microwave Theory Tech.*, vol. MTT-21, pp. 786–790, Dec. 1973.

[6] ——, "Hollow-cylinder waveguide isolators for use at millimeter wavelengths", *IEEE Trans. Microwave Theory Tech.*, vol. MTT-22, pp. 913–917, Nov. 1974.

[7] ——, "A millimeter-wave reflection-beam isolator," *IEEE Trans. Microwave Theory Tech.*, vol. MTT-23, pp. 506–508, June 1975.

[8] H. Jacobs and M. M. Chrepta, "Electronic phase shifter for millimeter-wave semiconductor dielectric integrated circuits," *IEEE Trans. Microwave Theory Tech.*, vol. MTT-22, pp. 411–417, Apr. 1974.

[9] N. Eberhardt, V. V. Horvath, and R. H. Knerr, "On plane and quasi-optical wave propagation in gyromagnetic media," *IEEE Trans. Microwave Theory Tech.*, vol. MTT-18, pp. 554–565, Sept. 1970.

[10] R. M. Knox and P. P. Toulios, "Integrated circuits for the millimeter through optical frequency range," in *Proc. Symp. on Submillimeter Waves*, Polytechnic Inst. of Brooklyn, pp. 497–516, 1970.

[11] E. A. J. Marcatili, "Rectangular waveguide and directional coupler for Integrated optics," *Bell Syst. Tech. J.*, vol. 48, pp. 2071–2102, Sept. 1969.

[12] W. V. McLevige, T. Itoh, and R. Mittra, "New waveguide structures for millimeter-wave and optical integrated circuits," *IEEE Trans. microwave Theory Tech.*, vol. MTT-23, pp. 788–794, Oct. 1975.

[13] I. Awai and T. Itoh, "Multilayered open dielectric waveguide with a gyrotropic layer," *Int. J. Infrared Millimeter Waves*, vol. 2, pp. 1–14, Jan. 1981.

[14] G. Forterre, B. Chiron, and L. Courtois, "A survey of broad band stripline ferrite isolators," *IEEE Trans. Magnetics*, vol. MAG-11, pp. 1279–1281, Sept. 1975.

[15] P. DeSantis, "A unified treatment of edge-guided waves," NRL Rep. 8158, Naval Res. Lab., Washington, DC 20375, Jan. 27, 1978.

[16] S. H. Talisa and D. M. Bolle, "On the modelling of the edge-guided mode stripline isolators," *IEEE Trans. Microwave Theory Tech.*, vol. MTT-27, pp. 584–591, June 1979.

[17] D. M. Bolle and S. H. Talisa, "The edge-guided mode nonreciprocal phase shifter," *IEEE Trans. Microwave Theory Tech.*, vol. MTT-27, pp. 878–882, Nov. 1979.

[18] D. F. Davidenko, "On a new method of numerical solution of systems of nonlinear equations," *Doklady Akad. Nauk S.S.S.R. (N.S.)*, vol. 88, pp. 601–602, 1953.

[19] P. T. Boggs, "The solution of nonlinear systems of equations by *A*-stable integration techniques," *SIAM J. Numer. Anal.*, vol. 8, pp. 767–785, 1971.

[20] L. F. Shampine, H. A. Watts, and S. Davenport, "Solving nonstiff ordinary differential equations—The state of the art," Sandia Lab. Rep. SAND 75-0182, 1974.

[21] G. E. Forsythe, M. A. Malcolm, and C. B. Moler, *Computer Methods for Mathematical Computations*. Englewood Cliffs, NJ. Prentice-Hall, 1977, ch. 6, pp. 129–147.

Salvador H. Talisa (M'76), for a photograph and biography please see page 923 of the September 1981 issue of this TRANSACTIONS.

Donald M. Bolle (S'56–M'57–SM'66), for a photograph and biography please see page 922 of the September 1981 issue of this TRANSACTIONS.